JOURNAL OF VIROLOGY, Jan. 2011, p. 98–111 Vol. 85, No. 1
0022-538X/11/$12.00 doi:10.1128/JVI.01902-10

Varicella-Zoster Virus Glycoprotein E Is a Critical Determinant of Virulence in the SCID Mouse-Human Model of Neuropathogenesis▽

Leigh Zerboni,[1]* Barbara Berarducci,[2] Jaya Rajamani,[1] Carol D. Jones,[3] James L. Zehnder,[3] and Ann Arvin[1]

Departments of Pediatrics, Microbiology and Immunology, Stanford University School of Medicine, Stanford, California 94305[1]; Department de Virologie, Institut Pasteur, Paris, France[2]; and Molecular Pathology Laboratory, Stanford University School of Medicine, Stanford, California 94305[3]

Received 8 September 2010/Accepted 13 October 2010

Varicella-zoster virus (VZV) is a neurotropic alphaherpesvirus. VZV infection of human dorsal root ganglion (DRG) xenografts in immunodeficient mice models the infection of sensory ganglia. We examined DRG infection with recombinant VZV (recombinant Oka [rOka]) and the following gE mutants: gEΔ27-90, gEΔCys, gE-AYRV, and gE-SSTT. gEΔ27-90, which lacks the gE domain that interacts with a putative receptor insulin-degrading enzyme (IDE), replicated as extensively as rOka, producing infectious virions and significant cytopathic effects within 14 days of inoculation. Since neural cells express IDE, the gE/IDE interaction was dispensable for VZV neurotropism. In contrast, gEΔCys, which lacks gE/gI heterodimer formation, was significantly impaired at early times postinfection; viral genome copy numbers increased slowly, and infectious virus production was not detected until day 28. Delayed replication was associated with impaired cell-cell spread in ganglia, similar to the phenotype of a gI deletion mutant (rOkaΔgI). However, at later time points, infection of satellite cells and other supportive nonneuronal cells resulted in extensive DRG tissue damage and cell loss such that cytopathic changes observed at day 70 were more severe than those for rOka-infected DRG. The replication of gE-AYRV, which is impaired for *trans*-Golgi network (TGN) localization, and the replication of gE-SSTT, which contains mutations in an acidic cluster, were equivalent to that of rOka, causing significant cytopathic effects and infectious virus production by day 14; genome copy numbers were equivalent to those of rOka. These experiments suggest that the gE interaction with cellular IDE, gE targeting to TGN sites of virion envelopment, and phosphorylation at SSTT are dispensable for VZV DRG infection, whereas the gE/gI interaction is critical for VZV neurovirulence.

Varicella-zoster virus (VZV) is a lymphotropic and neurotropic alphaherpesvirus and the etiological agent of varicella and herpes zoster. During primary infection, VZV virions gain access to sensory ganglion nerve cell bodies from either virion entry at nerve endings within cutaneous vesicular lesions or virus released by circulating infected T lymphocytes infiltrating ganglia (5). After the resolution of primary infection, VZV establishes a life-long latent infection within sensory nerve ganglia, from which it may reactivate to reinfect cutaneous sites. Thus, unlike infection of skin cells, VZV infection of neuronal ganglia requires neuronal cell survival to preserve host sites for the long-term establishment of latency.

Experimental systems for examining early stages of VZV neurotropism are limited by a marked human host cell restriction that precludes the productive infection of sensory nerve ganglia in small-animal models (5). Experimental infection of human dorsal root ganglion (DRG) xenografts maintained in severe combined immunodeficient (SCID) mice permits the examination of the interactions between VZV and human neurons, satellite cells, and other neural cells in intact ganglia (23). Using this model, we have defined critical steps in VZV replication and persistence in human neural tissue as well as a specific molecular requirement for VZV glycoprotein I (gI) in the transition to long-term persistence (24). In this report, we expand our examination of the capacity of VZV to replicate in human DRG by an evaluation of four recombinant viruses containing mutations in VZV glycoprotein E (gE).

VZV gE is a 623-amino-acid type I membrane protein encoded by open reading frame 68 (ORF68) and is the most abundant viral glycoprotein expressed on the surface of VZV-infected cells (5). The function of gE is best understood during VZV infection of epidermal cells in culture and in skin xenografts, where it plays a role in polykaryon formation (12–14). VZV gE has similarities to orthologous gE proteins in other human alphaherpesviruses with the important exception that gE is essential for VZV replication (5, 12). VZV gE is of interest as a potential neurovirulence factor in that herpes simplex virus (HSV) gE and pseudorabies virus (PRV) gE are implicated in the retrograde and anterograde axonal transport of virions during primary infection and reactivation from latency (6, 7, 16, 19, 20).

VZV gE contains a large N-terminal region that is not conserved in other alphaherpesviruses (1). Mutational analysis of the unique gE N-terminal region identified critical subdomains for VZV skin and T-cell tropism (1). Amino acids (aa) 51 to 187 are essential for viral replication in skin and T-cell xenografts; a partial deletion removing residues 28 to 90 in the gEΔ27-90 mutant abolished the gE interaction with cellular insulin-degrading enzyme (IDE), a putative VZV receptor (3). Despite an inability to bind IDE, gEΔ27-90 was able to replicate in skin, albeit with decreased cell-cell spread, and in T-cell

* Corresponding author. Mailing address: S-356, Stanford University School of Medicine, 300 Pasteur Dr., Stanford, CA 94305. Phone: (650) 723-6353. Fax: (650) 725-8040. E-mail: zerboni@stanford.edu.

▽ Published ahead of print on 20 October 2010.

FIG. 1. Diagram of VZV gE mutants in a recombinant Oka (rOka) strain. gEΔ27-90 contains a deletion of aa 28 to 90 in the unique N-terminal ectodomain, which abolishes interactions with cellular IDE. gEΔCys contains a deletion of the first cysteine-rich region in the ectodomain, which abolishes interactions with gI. The conserved C-terminal endodomain contains an AYRV TGN localization motif that was substituted for AARV in gE-AYRV; gE-SSTT contains a substitution of the acidic cluster SSTT with AAAA. TM, transmembrane.

xenografts (3). The ectodomain of VZV gE contains two cysteine-rich regions; the deletion of the first cysteine region in the gEΔCys mutant abolished the VZV gE and gI interaction and severely impaired cell-cell spread, viral entry, and replication in skin xenografts (2). The small gE endodomain contains motifs that may potentially function in the tissue-specific tropism of VZV; these include an AYRV motif (aa 568 to 571) that mediates gE trafficking to the *trans*-Golgi network (TGN) and an acidic cluster, SSTT (aa 588 to 601), that is phosphorylated by the VZV ORF47 protein kinase (9, 14). The AYRV motif is of interest in that it was demonstrated to be dispensable *in vitro*, but mutation reduced skin virulence and, to a lesser extent, replication in T cells *in vivo*. Mutation of the SSTT phosphorylation motif had no effect on replication *in vitro* or in skin and T-cell xenografts *in vivo* (14).

We examined gEΔCys and gEΔ27-90, which are ectodomain mutants, as well as gE-AYRV and gE-SSTT, with mutations in the endodomain, for their capacity to replicate and persist in human sensory ganglia using the SCID mouse-human DRG xenograft model. Taken together, analyses of these mutants demonstrate that requirements for gE functional domains differ in sensory nerve ganglia compared with skin and T cells and that the gE/gI interaction is a determinant of VZV neurovirulence.

MATERIALS AND METHODS

SCID mouse-human DRG mice. Human tissues were obtained in accordance with state and federal regulations. Animal protocols were approved by the Stanford University Administrative Panel on Laboratory Animal Care. SCID mice with human DRG xenografts were prepared as previously described (23). Briefly, human tissue (gestational age, 18 to 22 weeks) was provided by Advanced Bioscience Resources, Inc. (Alameda, CA). A single DRG (1 to 1.5 mm^3) was surgically implanted under the kidney capsule of sedated C.B-17 *scid*/*scid* mice (males 6 to 8 weeks of age) (Taconic Farms, Germantown, NY) by using a 16-gauge transplant needle. Within 8 weeks, DRG xenografts were sufficiently engrafted and ready for experimental infection with VZV gE mutants.

Viruses and cells. Recombinant Oka (rOka) and mutant viruses were generated by cosmid-based mutagenesis and transfected into MeWo (melanoma cell line) cells as previously described (11). gE is encoded by ORF68 in the short unique region of the VZV genome. A diagram of the relevant domains in VZV gE is provided in Fig. 1. Berarducci et al. previously described the construction of gEΔCys, which contains a deletion of residues 208 to 236 (2), and gEΔ27-90, which contains a deletion of residues 28 to 90 (3). The gEΔCys and gEΔ27-90 mutants were constructed by using recombinant parental Oka virus, which is derived from the clinical isolate (Oka strain) used to generate the varicella vaccine (15). Moffat et al. previously described the construction of gE-AYRV, in which the C-terminal TGN localization signal was changed from AYRV to AARV, as well as the generation of gE-SSTT, in which the serines and threonines in the SSTT acidic cluster were replaced with alanines (14). The gE-AYRV and gE-SSTT mutants were constructed by using recombinant vaccine Oka virus, which is derived from the varicella vaccine (11). In all experiments, intact rOka virus was used as the positive control. Previous work demonstrated that parental Oka and vaccine Oka viruses exhibit similar levels of growth in SCID-DRG xenografts (23). The construction of rOkaΔgI and kinetics of VZV DRG infection with this mutant were described previously (13, 24).

VZV infection of DRG xenografts. All recombinant viruses were propagated in human embryonic lung fibroblasts (HELF) for a minimum of three passages prior to the inoculation of DRG xenografts. Because of the cell-associated nature of VZV, the inoculants were freshly prepared from semiconfluent VZV-infected HELF monolayers with marked and equivalent-appearing cytopathic effects in 75% of cells. Viral titrations were performed on MeWo cells immediately following animal inoculation as previously described (23).

At 8 to 12 weeks after xenotransplantation, DRG were directly injected with VZV-infected HELF (10 μl; 27-gauge needle). Three to six implants were examined per VZV strain per time point. At the specified time points, tissues were removed from euthanized mice and immediately fixed in 4% paraformaldehyde for histological analysis or processed for an infectious virus release assay (IFA) and DNA/RNA extraction. For IFA, tissues were finely minced in phosphate-buffered saline (PBS), and one-half of the minced tissue lysate was cocultured with uninfected MeWo cells and passaged until viral plaques were observed or for at least six passages. For DNA extraction, minced tissue was treated with DNAzol (Invitrogen, Carlsbad, CA) according to the manufacturer's instructions. For RNA extraction, the minced tissue was placed into RNAlater solution (Invitrogen, Carlsbad, CA) for RNA stabilization and later extracted by using TRIzol reagent (Invitrogen, Carlsbad, CA) according to the manufacturer's instructions.

Quantitative real-time DNA PCR and RNA PCR. Quantitative real-time DNA PCR and RNA PCR were performed by using a 5′ exonuclease method as previously described (23). Briefly, dually labeled internally annealing probes (5′ 6-carboxyfluorescein [FAM] reporter fluorophore and 3′ TAMRA [6-carboxytetramethylrhodamine] quencher fluorophore) were detected in real time by using an ABI Prism 7700 instrument (Applied Biosystems, Foster City, CA). RNA samples were treated with DNase (DNA-free kit; Ambion, Inc., Austin, TX) prior to reverse transcription (RT) using the high-capacity cDNA Archive kit (Applied Biosystems, Foster City, CA). VZV probes for ORF31, ORF62, and ORF63 were synthesized and purified by Operon Technologies (Alameda, CA); sequences are provided in Table 1. The VZV genome copy number is reported as the number of VZV genomes per 10^5 human cells. A standard curve was generated by using probes for hypoxanthine phosphoribosyltransferase (HPRT) (RNA real-time PCR) or β-actin (DNA real-time PCR), and samples that contained less than 0.1 nanograms of human DNA or RNA were excluded from the analysis, as they were outside the standard curve limits.

VZV protein immunohistochemistry and confocal immunofluorescent microscopy. DRG xenografts were recovered from mice and immediately fixed in 4% paraformaldehyde and processed for paraffin embedding. For each virus examined, 2 to 4 infected DRG per time point were embedded into a single block. The embedded tissues were serially sectioned, generating approximately 150 slides/block, each with two 5-μm sections with 2 to 4 tissues/section. Every 10th slide (i.e., sections 10, 20, 30, and 40, etc.) was stained with hematoxylin and eosin (H&E) to identify regions containing islets of neuron-satellite cell complexes and to assess cytopathic effects throughout each DRG. Under every staining condition, 6 to 12 slides were examined, spanning regions containing neuron-satellite cell complexes (i.e., sections 11, 21, 31, and 41, etc.). Control slides were run in parallel.

Tissue sections were stained with antibody by using standard avidin-biotin-peroxidase immunohistochemistry using 3,3′-diaminobenzidine (DAB) substrate (Vector Laboratories, Burlingame, CA) or confocal immunofluorescent staining methods as previously described (23). Antibodies were used at dilutions recommended by the manufacturer. Monoclonal antibodies to the neural cell adhesion molecule (NCAM) and VZV gE were obtained from Millipore (Billerica, MA); anti-IDE antibody was obtained from Covance (Princeton, NJ). Polyclonal rabbit antiserum to VZV IE63 was kindly provided by William Ruyechan (State University of New York at Buffalo, Buffalo, NY). Polyclonal rabbit antisera to VZV gI (V67) and ORF29 were kindly provided by Saul Silverstein (Columbia University). Mouse monoclonal antibody to gI (HB6) was provided by Baghar Forghani (California State Department of Health Services). The generation of a

TABLE 1. Quantitative DNA and RNA real-time PCR probes and primer sequences

Primer or probe[a]	Sequence
VZV-gB primer (FRW)	5′-GATGGTGCATACAGAGAACATTCC-3′
VZV-gB primer (REV)	5′-CCGTTAAATGAGGCGTGACTAA-3′
VZV-gB probe	5′-(FAM)-TCCGCGCTGCAGGTTCCAGTAAT-(TAMRA)-3′
VZV-ORF62 primer (FRW)	5′-TCTTGTCGAGGAGGCTTCTG-3′
VZV-ORF62 primer (REV)	5′-TGTGTGTCCACCGGATGAT-3′
VZV-ORF62 probe	5′-(FAM)-TCTCGACTGGCTGGGACTTGCG-(TAMRA)-3′
VZV-ORF63 primer (FRW)	5′-ATTGAGGCGCCGAATGTTC-3′
VZV-ORF63 primer (REV)	5′-CTTCACCACCATCATCAGATACG-3′
VZV-ORF63 probe	5′-(FAM)-TTTGCATAGGAGCGCACTGGAATGTG-(TAMRA)-3′

[a] FRW, forward; REV, reverse.

rabbit polyclonal antibody to VZV ORF23 was previously described (4). IgG fractions were purified by using a Pierce protein A column (ThermoFisher Scientific, Waltham, MA). A hematoxylin blue nuclear counterstain was applied after chromogen development (Vector Laboratories, Burlingame, CA). Alexa 594 goat anti-mouse and anti-rabbit and Alexa 488 goat anti-rabbit and anti-mouse secondary antibodies were used for immunofluorescence and confocal microscopy (Invitrogen), along with Hoechst nuclear stain (Sigma). Slides were examined by using an AxioPlan 2 LSM 510 confocal microscope (Zeiss).

A method for the nonenzymatic pretreatment of formalin-fixed paraffin-embedded tissue sections (antigen retrieval) was employed to reverse cross-linkages between formalin and proteins (18). Briefly, 1,600 ml of citric acid-based antigen retrieval solution (pH 6.0) (Vector Laboratories) was brought to a full boil in a Mirro 4-quart pressure cooker on high heat. Deparaffinized and rehydrated tissue sections were immersed into the citrate buffer, and the lid was locked in place. Slides were maintained under heat and pressure until the pressure gauge maintained a steady rocking motion for 90 s. After 90 s, the pressure was released, and the slides were slowly cooled to room temperature.

Statistical analysis. Standard errors and *P* values for statistical significance were calculated by a Student's *t* test using Microsoft Excel software, version 11.2.

RESULTS

VZV gE interaction with cellular IDE is not required for VZV infection of DRG xenografts. To evaluate the requirement for the gE interaction with cellular IDE in VZV neurotropism, DRG xenografts were inoculated with 2.3×10^3 PFU of rOka and gEΔ27-90. At 14 days postinfection, 3.0×10^9 VZV genome copies per 10^5 human cells were detected in rOka-infected implants by using the ORF31 probe; copy numbers decreased significantly, as expected, to 3.5×10^8 copies/10^5 cells and 8.3×10^7 copies/10^5 cells by 28 and 56 days postinfection, respectively, indicating a transition to VZV persistence (day 14 versus day 28; $P = 0.04$) (Fig. 2). A similar trend was observed by using probes to ORF62 and ORF63, with a 100-fold decrease in VZV genome copy numbers between 14 days and 56 days postinfection (data not shown). The gEΔ27-90 mutant exhibited a trend similar to that of rOka at the early time point, with 5.6×10^8 VZV genome copies/10^5 cells at 14 days postinfection, which decreased significantly to 1.3×10^7 genome copies/10^5 cells by day 28 ($P = 0.04$) (Fig. 2). VZV genome copy numbers were reduced 5-fold in DRG infected with gEΔ27-90 compared with rOka virus at 14 days postinfection, but this was not a statistically significant difference. A similar trend was observed by using probes for ORF62 and ORF63 (data not shown).

Infectious virus production from infected DRG homogenates was assessed; aggregate data are provided in Table 2. Infectious virus was recovered from all 3 DRG xenografts infected with rOka and gEΔ27-90 at 14 days postinfection and from 1/3 and 0/3 DRG xenografts infected with rOka and gEΔ27-90 at 28 days postinfection, respectively. These data suggest that the VZV gE interaction with cellular IDE is dispensable for the VZV infection of DRG xenografts as well as for the transition to viral persistence.

Deletion of the first cysteine-rich domain in gE alters the kinetics of VZV replication in DRG xenografts. In the same experiment described above, DRG xenografts were inoculated with 8.5×10^3 PFU gEΔCys virus. VZV genome copy numbers were significantly reduced in DRG xenografts inoculated with gEΔCys at 14 days postinfection compared with those of rOka, despite a 3.7-fold difference in the titers of the virus inocula; 1.5×10^8 VZV genome copies per 10^5 human cells were detected by using the ORF31 probe ($P = 0.02$ for rOka versus gEΔCys on day 14) (Fig. 2). Moreover, the trend for decreasing numbers of VZV genomes between days 14 and 28, observed

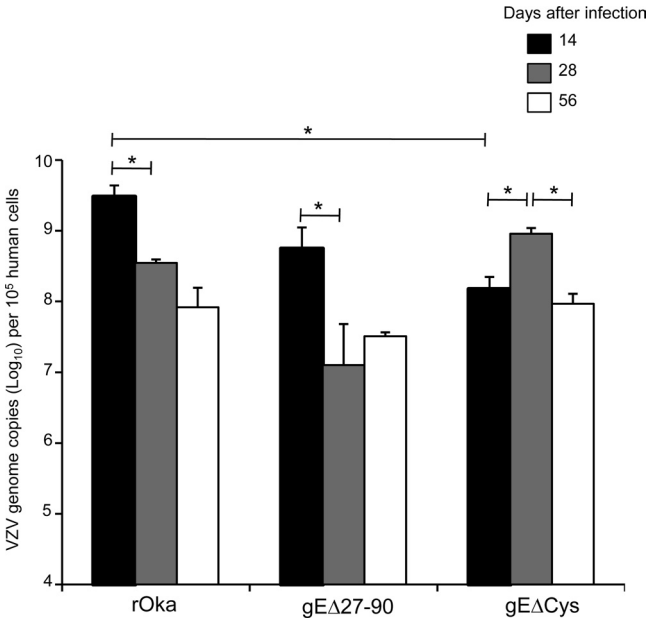

FIG. 2. VZV genome copy numbers in DRG xenografts infected with rOka, gEΔ27-90, and gEΔCys determined by using quantitative real-time PCR. VZV genome copy numbers in DRG infected with rOka, gEΔ27-90, and gEΔCys were assessed by quantitative real-time PCR using probes for ORF31 (gB) as well as ORF62 and ORF63 (not shown). DRG were evaluated at 14, 28, and 56 days postinfection. Three to five xenografts were tested at each time point. VZV genome copy numbers are reported as mean copies per 10^5 human cells ± standard errors. Bars with asterisks indicate *P* values of <0.05.

TABLE 2. Recovery of infectious virus from DRG xenografts

Virus	No. of infectious xenografts/total no. of xenografts on day[a]:		
	14	28	56
rOka	3/3	1/3	0/3
rOka gE-ΔCys	0/3	3/3	0/3
rOka gE-Δ27-90	3/3	0/3	ND
rOka gE-AYRV	3/4	0/4	ND
rOka gE-SSTT	2/4	0/4	ND

[a] ND, not determined.

for DRG xenografts infected with rOka and gEΔ27-90, was not observed. VZV genome copy numbers were increased at 28 days postinfection in DRG infected with gEΔCys (9.1×10^8 genome copies per 10^5 cells; $P = 0.01$ compared to day 14) and then reduced by day 56 postinfection (9.3×10^7 genome copies/10^5 cells; $P = 0.01$ compared to day 28) (Fig. 2). The increase in VZV genome copy numbers at day 28 correlated with the production of infectious virus, which was recovered in all three DRG homogenates infected with gEΔCys, whereas no infectious virus was recovered at days 14 and 56 (Table 2). Taken together, the detection of increased VZV genome copy numbers by day 28 and infectious virus suggests that the abrogation of the interaction between gE and gI delays but does not circumvent lytic VZV replication in DRG xenografts.

Histopathology of DRG infected with rOka and gEΔ27-90. To evaluate the histopathological effect of DRG infection with VZV rOka and gEΔ27-90, DRG were inoculated with 3.1×10^3 PFU rOka and 2.6×10^3 PFU gEΔ27-90. DRG xenografts were removed, fixed, and processed for histological analysis at 14 and 56 days postinfection. Typical histological features of DRG include clusters of small- and large-diameter neuronal cell bodies, each with a prominent nucleus, in association with satellite cells that ring the neuronal cytoplasm (Fig. 3A, black arrow). These neuron-satellite cell complexes are surrounded by a supportive matrix of Schwann cells and fibroblasts with interwoven collagen and neural bundles (Fig. 3A, white arrow). The cytopathic effect of acute, productive VZV infection in rOka-infected xenografts was consistent with previous observations (24). At 14 days postinfection, rOka-infected DRG exhibited marked cytopathic changes in which many neurons appeared to have a contracted cytoplasm (Fig. 3B, black arrow), inclusions, or vacuolizations (Fig. 3B, white arrow), and many satellite cells had irregular morphology. A VZV immediate-early protein (IE63), which indicates VZV infection, was detected within satellite cells and neuronal cell bodies as well as along nerve bundles and within nonneuronal cells (Fig. 3C). By 56 days postinfection, VZV IE63 expression was absent (Fig. 3D). Clusters of normal-appearing neuron-satellite cell complexes within an organotypic supportive matrix remained.

DRG xenografts infected with gEΔ27-90 had a phenotype similar to that of rOka-infected DRG. Consistent with the detection of large numbers of VZV genomes and the production of infectious virus, at 14 days postinfection with gEΔ27-90, neurons and satellite cells exhibited a marked cytopathic effect, including cytoplasmic contraction and inclusion bodies. The VZV IE63 protein was expressed in neurons and satellite cells as well as along nerve bundles in DRG xenografts (Fig. 3E). By 56 days postinfection, the marked cytopathic effect had resolved, and regions of the tissue retained organotypic features of normal DRG; IE63 protein expression was absent (Fig. 3F). To verify that cellular IDE is expressed in SCID mouse-human DRG xenografts, sections of infected and uninfected DRG were stained with anti-IDE antibody. Cellular IDE was detected within neurons as well as in satellite cells and other supporting cell types within VZV-infected human DRG xenografts (Fig. 3G). No staining was observed when the primary antibody was substituted for rabbit serum (Fig. 3H).

Localization of IE63 and gE in DRG infected with rOka and gEΔ27-90. In a previous report, we quantified IE63 expression patterns within individual neuron-satellite cell complexes during peak replication (17). IE63 was most often observed within both the neuron and investing satellite cells; rarely, IE63 was observed only in satellite cells (5%) or neurons (<1%). We observed a similar IE63 expression pattern for rOka-infected DRG in these experiments. The IE63 protein was observed primarily within both neurons and investing satellite cells at 14 days after infection and only rarely in neurons alone or satellite cells (Fig. 4A). VZV gE expression was observed within individual neuron-satellite cell complexes in which the IE63 protein was also detected and along nerve bundles. Within IE63-positive neuron-satellite cell complexes, gE was localized primarily to the neuronal cellular membranes as well as demarcating individual satellite cell boundaries (Fig. 4B, short white arrow). Cytoplasmic gE was often observed and appeared to be contained within discrete compartments (Fig. 4B, C, and C*, short arrow). gE was also detected within some neuron-satellite cell complexes in the absence of IE63 expression or when IE63 expression was dim (Fig. 4E, long white arrow, and F*, short arrow). In those cells, gE staining was dense, and the boundary between the neuron and investing satellite cells was poorly defined; staining with Hoechst dye was often absent or dim, suggesting impending cell death.

The membrane localization of gE in IE63-positive neuron-satellite cell complexes in DRG infected with gEΔ27-90 was similar to that in DRG infected with rOka; gE was membrane associated and was also present within the neuronal cytoplasm. However, in IE63-negative or dim neuron-satellite cell complexes, dense membrane expression of gE was not as apparent (Fig. 4H, long arrow, and I*, short arrow). gE was less evenly distributed along cellular membranes, and cytoplasmic staining was often observed and localized within the perinuclear zone.

Histopathology of DRG infected with gEΔCys. DRG xenografts inoculated with gEΔCys (4.4×10^3 PFU) were evaluated at 14, 44, 56, and 70 days postinfection. In a separate experiment, DRG xenografts were inoculated with 2.6×10^4 PFU and evaluated at 28 days postinfection. The results are presented together in Fig. 5. Whereas infection with rOka resulted in pronounced cytopathic effects at 14 days postinfection, DRG xenografts infected with gEΔCys had no obvious indicators of an infectious process. Cytoplasmic contraction was observed within a few neuron-satellite cell complexes (Fig. 5A, black arrow), but IE63 immunoreactivity was absent (Fig. 5B). By 28 days after infection, a cytopathic effect was observed, indicating lytic infection, but only within a few isolated neuron-satellite cell complexes despite the use of a higher-titer inoculum.

At day 44, clusters of satellite cells that formed rosettes,

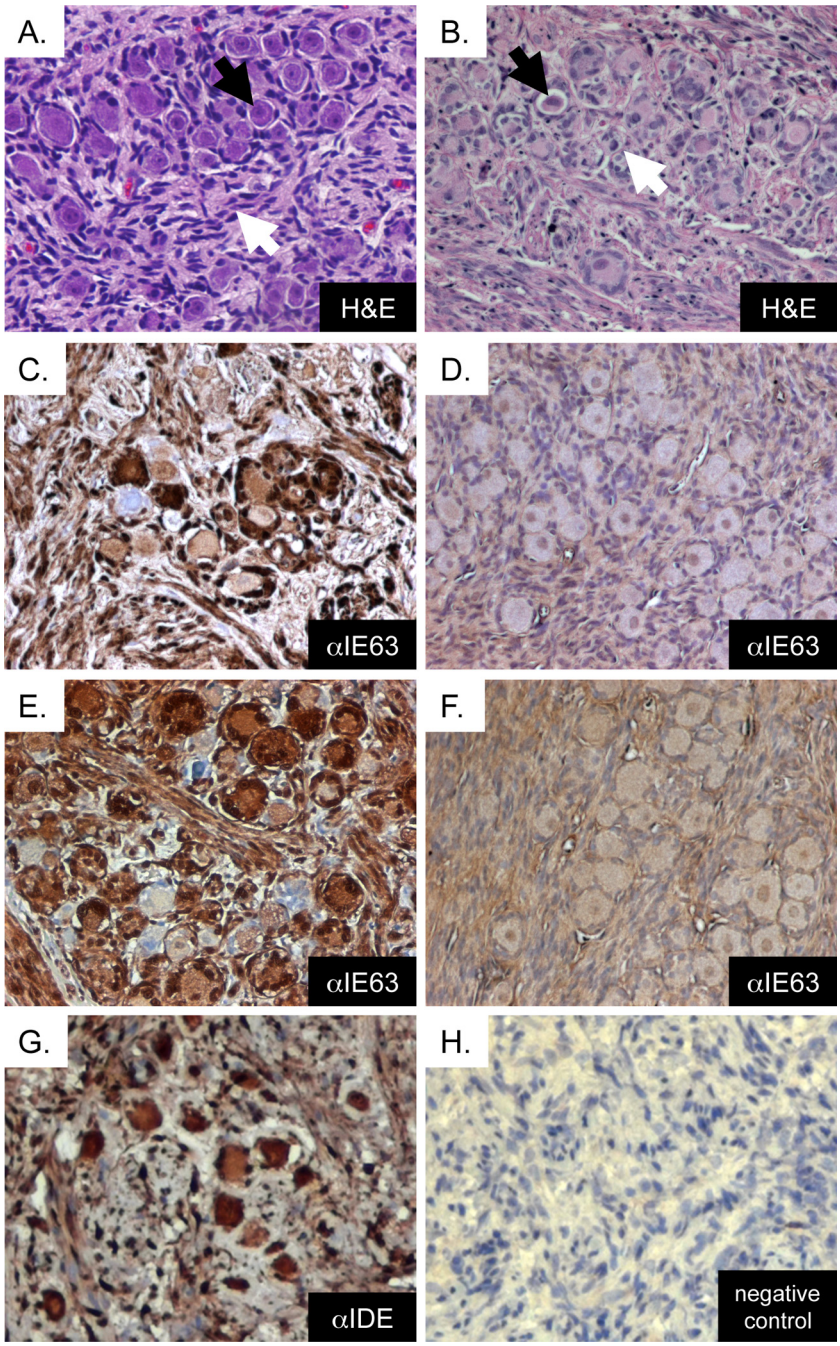

FIG. 3. Cytopathic effects of DRG xenograft infection with rOka and gEΔ27-90. (A) Uninfected DRG xenograft 8 weeks posttransplantation, with H&E staining (magnification, ×200). The black arrow indicates a neuron-satellite cell complex, and the white arrow indicates axons. (B) rOka-infected xenograft 14 days postinfection, with H&E staining (magnification, ×200). The black arrow denotes a contracted cytoplasm, and the white arrow denotes cytoplasmic inclusions that are typically observed during lytic replication. (C and D) rOka-infected xenograft at 14 days (C) and 56 days (D) postinfection, stained with anti-IE63 using DAB (brown) chromogen and counterstained with hematoxylin (magnification, ×200). (E and F) gEΔ27-90-infected xenograft at 14 days (E) and 56 days (F) postinfection, stained with anti-IE63 using DAB (brown) chromogen and counterstained with hematoxylin (magnification, ×200). (G) rOka-infected xenograft at 14 days postinfection, stained with antibody to cellular IDE using DAB (brown) chromogen and counterstained with hematoxylin (magnification, ×200). (H) Negative-control slide (no primary antibody).

which indicate the replacement of damaged neurons with proliferating satellite cells, referred to as nodules of Nageotte, were abundant; many neurons contained condensed nuclear material, and fibrosis was observed (Fig. 5C, black arrows). VZV IE63 protein expression was observed within many neuron-satellite cell complexes and especially within nonneuronal cells (Fig. 5D). VZV ORF23, a capsid protein, and VZV ORF29, a single-stranded DNA binding protein, were detected

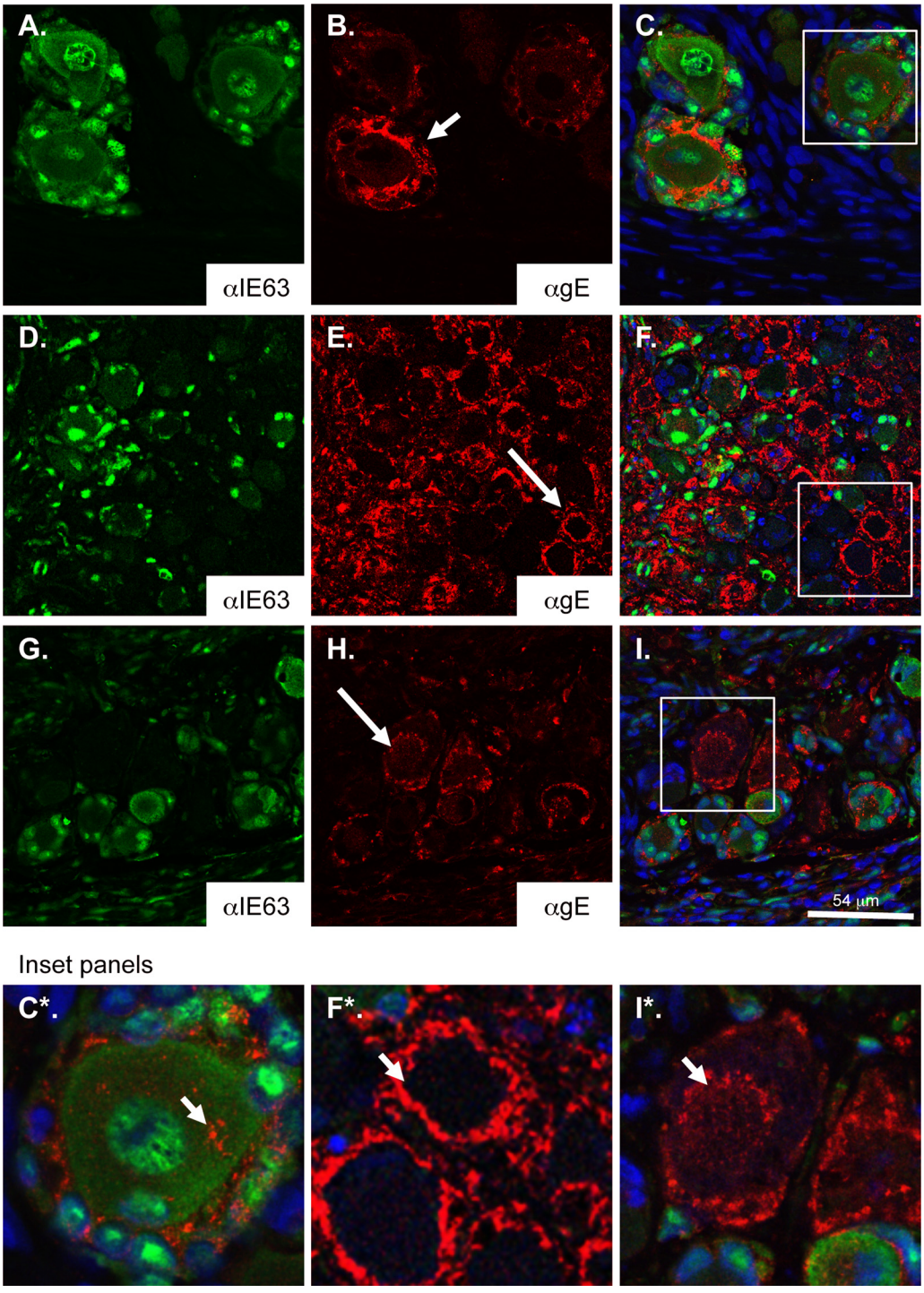

FIG. 4. Localization of gE in DRG infected with rOka and gEΔ27-90. Shown are rOka-infected (A to F) or gEΔ27-90-infected (G to I) DRG xenografts 14 days after infection, stained with anti-IE63 (A, D, and G) or anti-gE (B, E, and H). (C, F, and I) Overlay images with Hoechst nuclear stain. (C*, F*, and I*) Enlargements of inset panels. The arrow in B shows membrane gE staining, and the small arrow in C* shows cytoplasmic gE staining in rOka-infected DRG. Arrows in E and F* show dense gE membrane staining. The arrow in H and small arrow in I* denote cytoplasmic accumulation of gE in gEΔ27-90-infected neurons. Magnifications, ×200 (D to F) and ×400 (A to C and G to I).

in neurons and satellite cells, indicating ongoing lytic infection (Fig. 5E and F).

By day 56, islets of neurons remained in only 1 of 9 DRG; these islets contained many neuron-satellite cell complexes that appeared normal, but the surrounding tissue exhibited extensive damage and cell loss (Fig. 5G, black arrows). Extensive acellular fields with fibrosis and remnants of neuron-satellite cell complexes were observed in 8 of 9 DRG infected

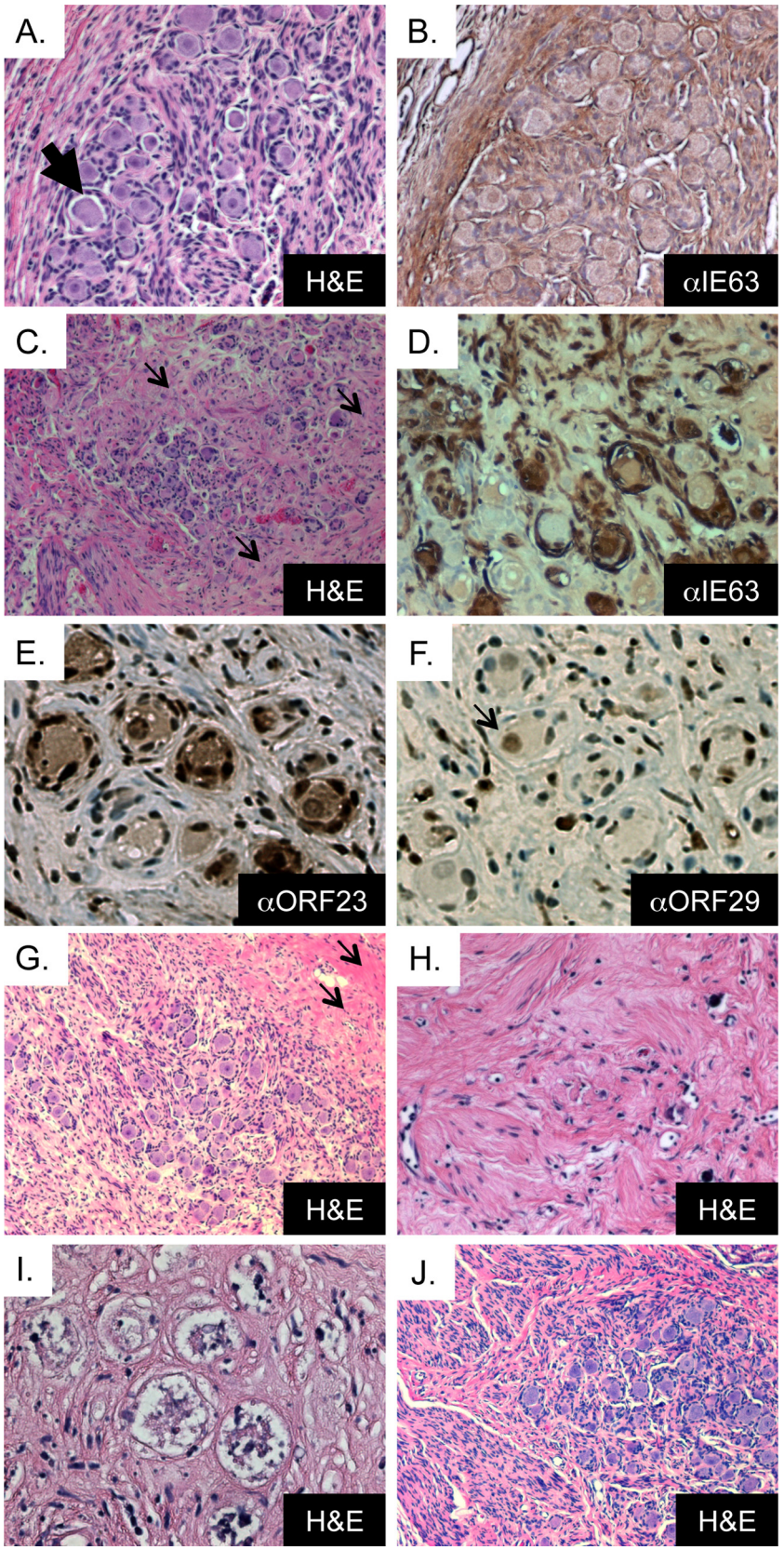

FIG. 5. Cytopathic effect of xenograft infection with rOka gEΔCys. (A) gEΔCys-infected xenograft at 14 days postinfection, with H&E staining (magnification, ×200). The arrow denotes a contracted cytoplasm. (B) gEΔCys-infected xenograft at 14 days postinfection, stained with anti-IE63 using DAB (brown) chromogen and counterstained with hematoxylin (magnification, ×200). (C) gEΔCys-infected xenograft at 44 days postin-

with gEΔCys (Fig. 5H and I). The overall extent of DRG damage, i.e., neuronal cell loss, rosetting satellite cells, and fibrosis, was more extensive in DRG infected with gEΔCys than in rOka-infected DRG examined at 56 and 70 days after infection (compare Fig. 5H, I, and J).

Aberrant expression of gE and gI in DRG infected with gEΔCys. We assessed the expression and subcellular localization of gE and gI in the absence of a gE/gI interaction by confocal immunofluorescent microscopy of DRG using a rabbit polyclonal antibody to gI and a mouse monoclonal antibody to gE. In a previous report, we described a patchy, uneven distribution of gE on cellular membranes of cultured melanoma cells infected with the gEΔCys mutant compared with rOka (2). In rOka-infected DRG (evaluated at 14 days postinfection), the gE protein (Fig. 6B) was readily detected and strongly colocalized with gI (Fig. 6A) along plasma membranes, with minimal cytoplasmic staining (Fig. 6A to C). In contrast, both gE and gI were absent from cellular membranes in DRG xenografts infected with gEΔCys and evaluated at 44 days postinfection (Fig. 6D to F). gE and gI did colocalize, but staining was observed only in rare cells and was confined to the cytoplasm (Fig. 6F). This staining pattern is dissimilar to that found in our previous observations of cultured melanoma cells and suggests a tissue-specific requirement for gI in gE neuronal expression. Sections were also stained with a mouse monoclonal antibody to gI (Fig. 6H) and a polyclonal rabbit antibody to IE63 (Fig. 6G). In rOka-infected cells (14 days after infection), gI was detected along neuronal membranes (Fig. 6H and I). However, in gEΔCys-infected DRG (44 days after infection), dim cytoplasmic staining was observed, which was not significantly different from results using nonimmune rabbit serum (Fig. 6K).

Absence of gE/gI interaction disrupts VZV-induced fusion of membranes in neuron-satellite cell complexes. In a previous report, we provided ultrastructural evidence for polykaryon formation between neuronal and satellite cell membranes and demonstrated that the discontinuity of neural cell adhesion molecule (NCAM) membrane expression is a reliable marker for the fusion of neuronal membranes (17). We examined the requirement for the gE/gI interaction for VZV-induced membrane fusion by staining DRG sections for IE63, as a marker of VZV infection, and examining the NCAM plasma membrane distribution. In uninfected DRG sections, NCAM is evenly distributed along the inner margin of the neuronal cell cytoplasm and between adjacent satellite cells; NCAM staining clearly demarcates the boundaries between satellite cells and the neuronal cytoplasm (Fig. 7A). In contrast, NCAM expression within the inner membrane was absent, and overall expression was dim and discontinuous in a significant proportion (approximately 70%) of rOka-infected neuron-satellite cell complexes (14 days after infection) that had neuronal cytoplasmic IE63 expression (Fig. 7B to D, long arrow). The absence of an apparent separation between the neuronal cell cytoplasm and investing satellite cells indicates a fusion of neuronal membranes to form a polykaryon. In neuron-satellite cell complexes in which IE63 staining was restricted to investing satellite cells, NCAM staining along the inner margin of the neuronal cell cytoplasm was intact (Fig. 7B to D, short arrow).

The pattern of NCAM distribution in rOka-infected neuron-satellite cell complexes was compared with the NCAM distribution patterns in rOkaΔgI-infected DRG (70 days after infection) and gEΔCys-infected DRG (44 days after infection) in neurons that showed cytoplasmic IE63 staining. In IE63-positive neurons infected with rOkaΔgI, the NCAM distribution was remarkably similar to that of uninfected DRG. In most IE63-positive neurons, NCAM expression was evenly distributed along the inner margin of the neuronal cell cytoplasm and demarcated the boundaries between satellite cells (Fig. 7E to G). Discontinuous patchy NCAM staining was present in only a small proportion of neurons infected with rOkaΔgI. NCAM expression was also continuous in neuron-satellite cell complexes in which the IE63 signal was confined to satellite cells (Fig. 7H to J). Clearly defined NCAM-stained boundaries were readily observed between neuronal and satellite cell cytoplasms in neurons infected with gEΔCys, even when IE63 staining of the neuronal cell cytoplasm was apparent (Fig. 7K to M, short arrows).

Taken together, these observations indicate that the absence of a gE/gI interaction inhibits the VZV-induced fusion of neuronal membranes with adjacent satellite cells, which is a hallmark of VZV infection of DRG, and that the deletion of the first cysteine-rich domain of gE restricts the capacity for spread within the infected ganglion. Interestingly, whereas the restriction of IE63 expression to satellite cells is uncommon in DRG infected with intact rOka, this pattern was frequently observed for tissues infected with rOkaΔgI (Fig. 7I) and, to a lesser extent, gEΔCys (Fig. 6J and 7L).

Disruption of the AYRV or SSTT functional motif does not impair VZV replication in DRG xenografts. To evaluate the contributions of gE endodomain functional motifs to the facilitation of VZV neurotropism, DRG xenografts were inoculated with rOka, gE-AYRV, and gE-SSTT mutant viruses (2.3×10^2 PFU, 5.3×10^2 PFU, and 4.3×10^2 PFU, respectively). At 14 days after infection, 5.7×10^7 genome copies/10^5 cells of ORF31 were detected in rOka-infected implants, which dropped significantly to 1.4×10^6 copies/10^5 cells by day 56 ($P \leq 0.05$) (Fig. 8A). The gE-AYRV and gE-SSTT mutants exhibited a similar trend, with 1.8×10^7 copies/10^5 cells at day 14 and 3.0×10^5 copies/10^5 cells at day 56 for rOka gE-AYRV and 1.9×10^7 copies/10^5 cells at day 14 and 1.8×10^6 copies/

fection, with H&E staining (magnification, ×100). (D) gEΔCys-infected xenograft at 44 days postinfection, stained with anti-IE63 using DAB (brown) chromogen and counterstained with hematoxylin (magnification, ×200). (E) gEΔCys-infected xenograft at 44 days postinfection, stained with anti-ORF23 using DAB (brown) chromogen and counterstained with hematoxylin (magnification, ×200). (F) gEΔCys-infected xenograft at 44 days postinfection, stained with anti-ORF29 using DAB (brown) chromogen and counterstained with hematoxylin (magnification, ×200). The black arrow denotes a positive neuronal cell nucleus. (G) gEΔCys-infected xenograft at 56 days postinfection, with H&E staining (magnification, ×100). (H and I) Extensive fibrosis and remnants of neuron-satellite cell complexes in a gEΔCys-infected xenograft at 56 days after infection, with H&E staining (magnification, ×200). (J) rOka-infected xenograft at 70 days postinfection, with H&E staining (magnification, ×100). Small black arrows in C and E denote fibrotic areas.

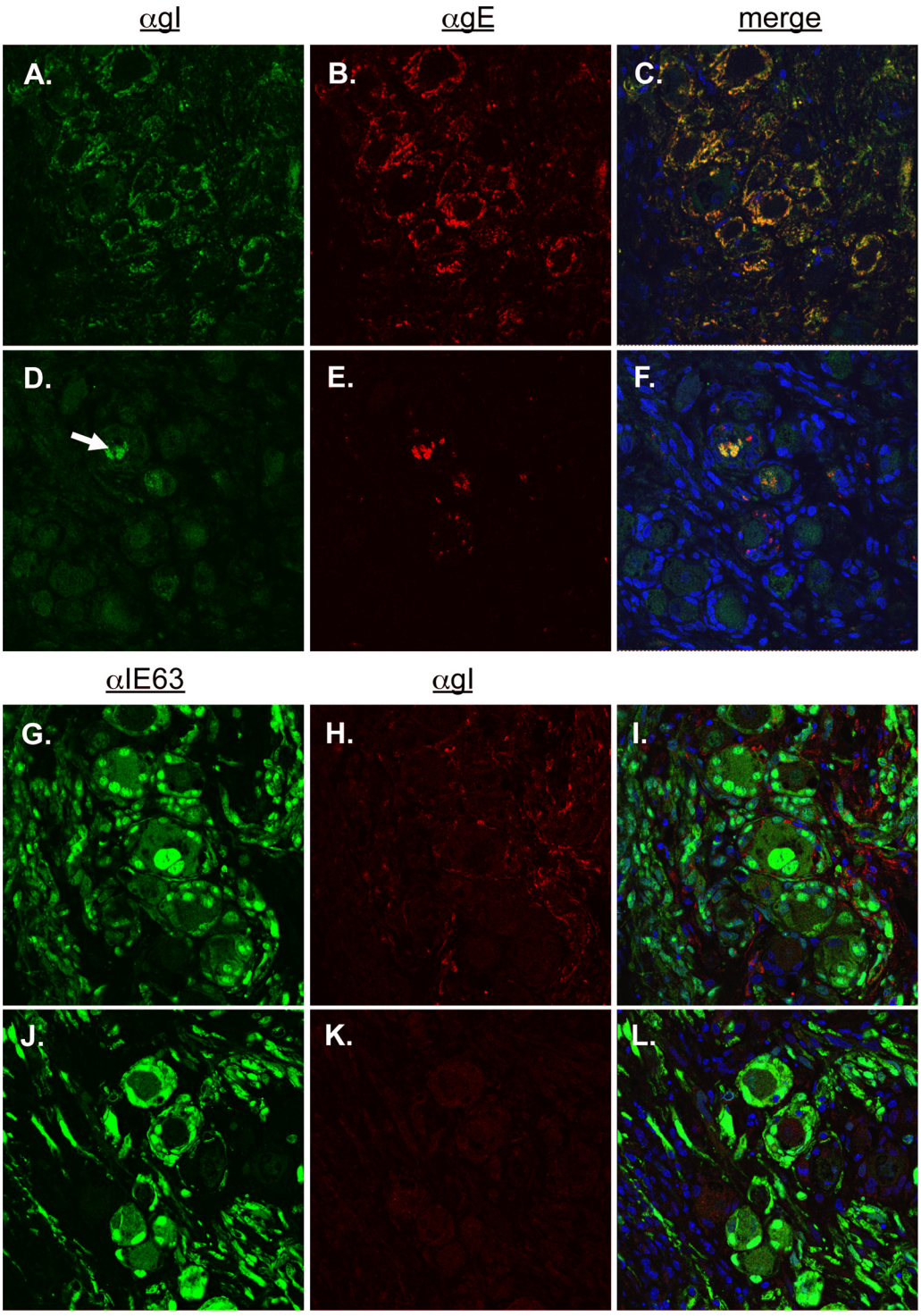

FIG. 6. Aberrant expression of VZV gE and gI in gEΔCys-infected xenografts. (A to F) rOka-infected DRG xenograft at 14 days postinfection (A to C) or gEΔCys-infected xenografts at 44 days postinfection (D to F), stained with rabbit polyclonal antibody to gI (green) (A and D) and mouse monoclonal antibody to gE (red) (B and E). Merged images with blue nuclear stain (Hoechst) are shown in C and F. Magnification, ×200. (G to L) rOka-infected DRG xenograft at 14 days postinfection (G to I) or gEΔCys-infected xenografts at 44 days postinfection (J to L), stained with rabbit polyclonal antibody to IE63 (green) (G and J) and mouse monoclonal antibody to gI (red) (H and K). Merged images with blue nuclear stain (Hoechst) are shown in I and L. Magnification, ×400.

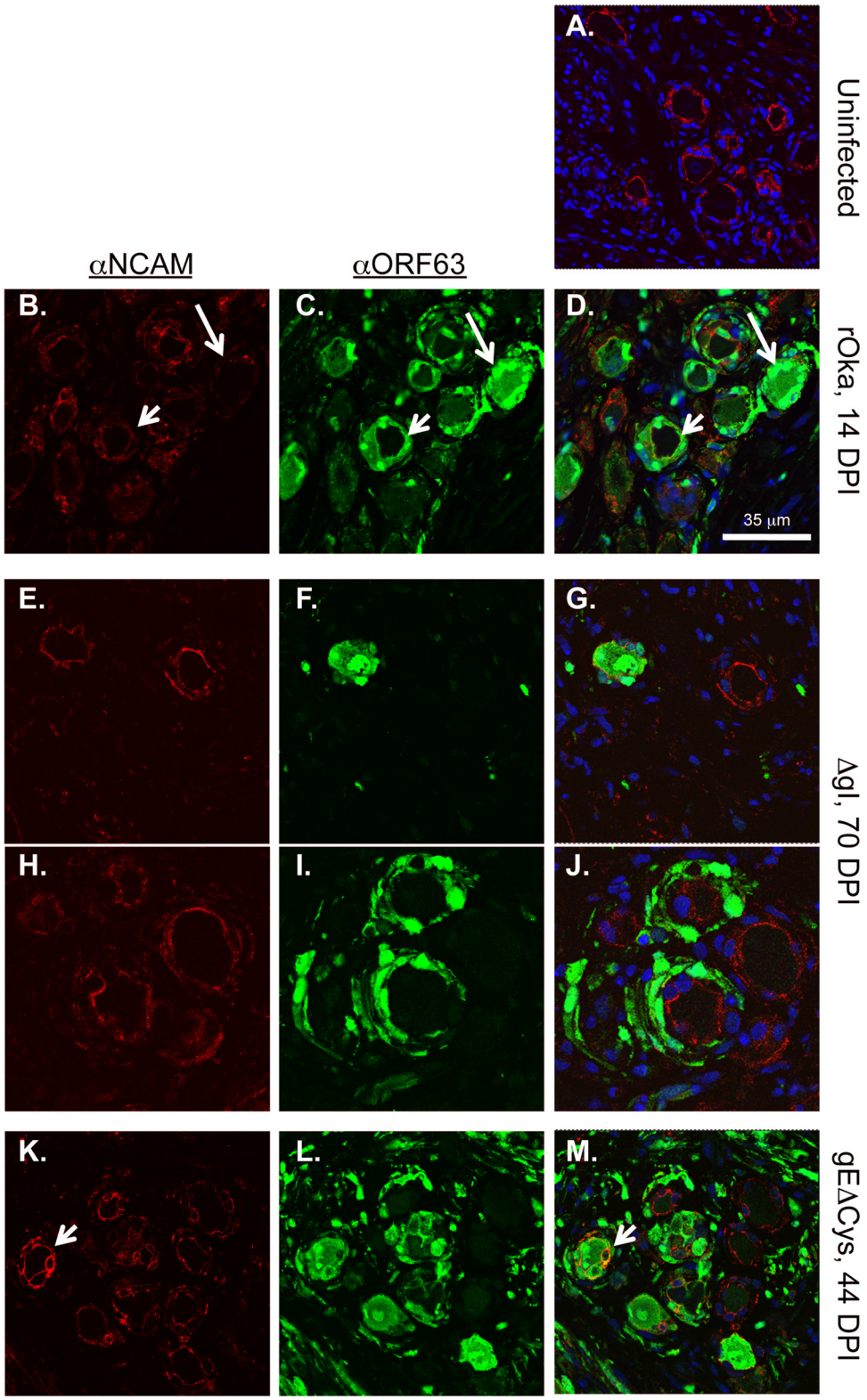

FIG. 7. Inhibition of VZV-induced fusion in gEΔCys- and ΔgI-infected DRG xenografts. (A) Uninfected DRG xenograft stained with anti-NCAM and Hoechst nuclear stain. (B to J) rOka-infected xenograft at 14 days postinfection (DPI) (B to D), ΔgI-infected DRG xenograft at 70 days postinfection (E to J), and gEΔCys-infected DRG at 44 days after infection (K to M). B, E, H, and K are stained with NCAM; C, F, I, and L are stained with anti-IE63; and merged images with Hoechst nuclear stain are shown in D, G, J, and M. Magnification, ×400.

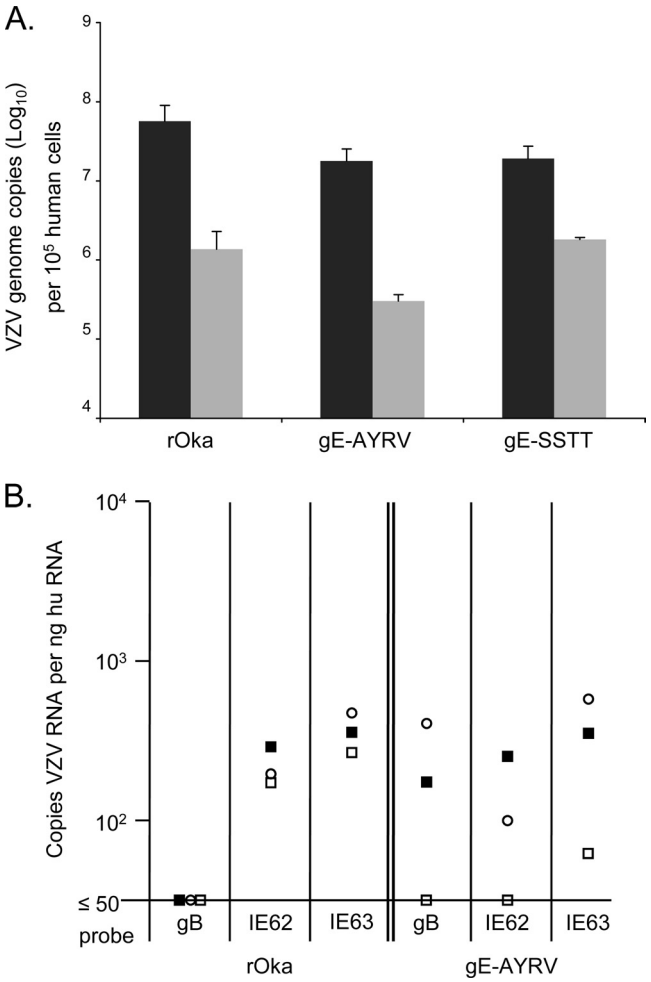

FIG. 8. VZV genome copy numbers in DRG xenografts infected with rOka, gE-AYRV, and gE-SSTT. (A) VZV genome copy numbers were assessed by quantitative real-time PCR using a probe for ORF31 at 14 and 56 days postinfection (black bars and gray bars, respectively). Three to five xenografts were tested at each time point. VZV genome copy numbers are reported as mean copies per 10^5 human cells ± standard errors. *P* values were determined by using a Student's *t* test. (B) VZV transcripts for ORF31, ORF62, and ORF63 assessed by quantitative real-time RT-PCR at 56 days postinfection in DRG xenografts infected with rOka and gE-AYRV. Symbols represent individual DRG. Results are reported as mRNA copies per nanogram of human mRNA (HPRT control). DRG RNA preparations that contained <0.1 ng of huRNA per well or <50 copies per DRG were excluded from the analysis, as they were outside the limits of the standard curve.

10^5 cells at day 56 for rOka gE-SSTT (Fig. 8A). The difference between the VZV genome copy numbers at day 14 and day 56 represents a significant reduction for rOka as well as the two gE C-terminal mutants ($P \leq 0.05$); however, differences between rOka and the C-terminal mutants were not significant. A similar trend was observed when the ORF62 probe was used to measure genome copy numbers (data not shown). Infectious VZV was recovered from 3/3 rOka-infected implants, from 3/4 gE-AYRV-infected implants, and from 2/4 gE-SSTT-infected implants at day 14 (Table 2). No virus was recovered from gE-AYRV- and gE-SSTT-infected DRG xenografts at 28 days postinfection. Virus was recovered in 1/3 rOka-infected xenografts at 28 days postinfection (Table 2).

Disruption of the AYRV functional motif alters transcriptional repression of gB. Quantitative RT-PCR was performed on RNA extracted from rOka- and gE-AYRV-infected DRG xenografts at 56 days postinfection to measure the expression of viral mRNAs corresponding to late (gB) and immediate-early (IE62 and IE63) gene products. Transcripts for gB were not detected in rOka-infected DRG, but IE62 and IE63 mRNAs were detected at 218 ± 42 copies per nanogram human RNA (huRNA) and 798 ± 245 copies per nanogram human RNA, respectively (Fig. 8B). In DRG xenografts infected with gE-AYRV, transcripts for gB as well as those for IE62 and IE63 were detected. The levels of IE62 and IE63 mRNA expression in gE-AYRV-infected implants were reduced compared to that in rOka-infected DRG (132 ± 93 IE62 copies per ng human RNA and 368 ± 260 IE63 copies per ng human RNA) but not significantly (Fig. 8B). In previous work, we reported that VZV persistence in DRG was associated with ORF63 transcription and some ORF62 transcription as well as the suppression of gB gene transcription (23). The low level of gB transcripts that remained detectable in gE-AYRV-infected DRG may reflect a slight delay in viral replication and transition to a persistent state.

Localization of gE in DRG infection with gE-AYRV. Histological analysis of gE-AYRV-infected DRG sections at 14 days after infection showed cytopathic changes similar to those observed for rOka-infected DRG, such as cytoplasmic inclusions and contracted cytoplasm in neurons (Fig. 9A, white arrow). To assess the expression and trafficking of gE during acute infection with gE-AYRV, we examined sections by confocal immunofluorescence microscopy using antibodies to gE and IE63. As described above, gE expression was localized primarily to the plasma membrane of neurons and satellite cells in rOka-infected DRG, with some staining within the neuronal cytoplasm (Fig. 4B and E). In gE-AYRV-infected IE63-positive neurons, gE membrane staining was less evenly distributed than in rOka-infected neurons, but cytoplasmic staining was similar (compare Fig. 4 and 9C and D). The dense gE membrane expression in IE63-negative/Hoechst-negative neurons, which was observed for DRG infected with rOka and gEΔ27-90 and indicates impending cell death, was only rarely observed, which provides further evidence for a slight delayed-growth phenotype.

DISCUSSION

We analyzed the role of VZV gE in neurotropism and neuropathogenesis within the biologically relevant context of viral replication in human sensory ganglia *in vivo*. VZV infection in DRG xenografts with intact rOka reaches peak titers after 14 days. Infectious virus and VZV immunoreactivity are absent by day 28; however, genomes persist in ganglionic tissues that exhibit moderate fibrosis but contain normal-appearing areas with neurons and investing satellite cells (23). The transition from acute replication to viral persistence occurs in the absence of adaptive immune responses, which SCID mice lack (23). This process suggests that VZV has evolved the capacity to restrict VZV neurovirulence during primary infection so that neuronal sites for latency persist (23). The ability to resist

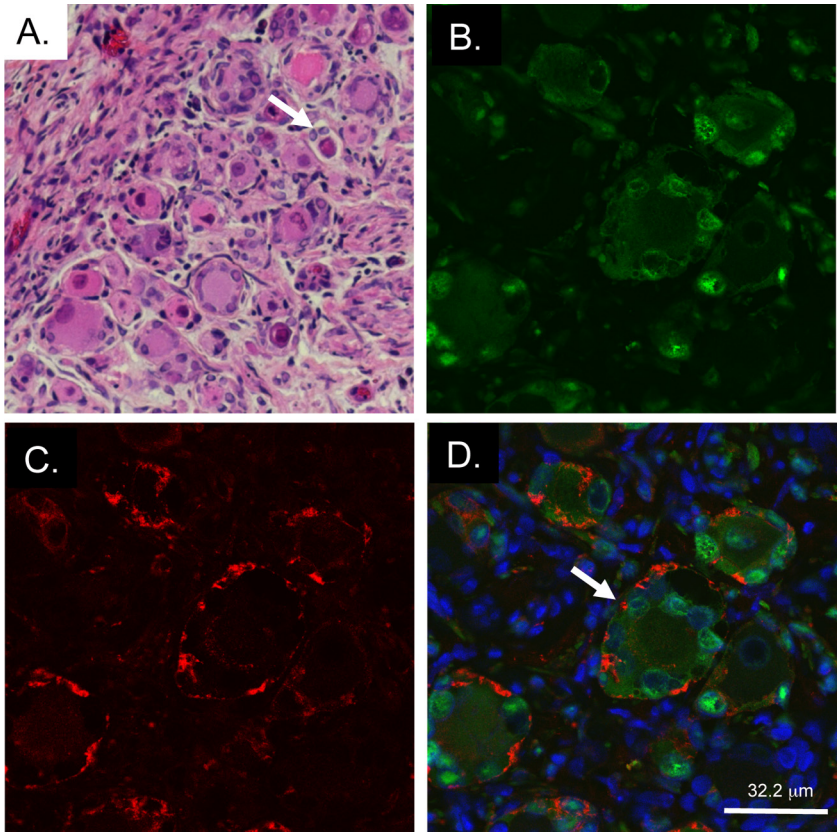

FIG. 9. Histopathological effects of DRG xenograft infection with gE-AYRV. (A) gE-AYRV-infected xenograft at 14 days postinfection, with H&E staining (magnification, ×200). The white arrow indicates a cytopathic effect in the neuron, i.e., contracted cytoplasm and inclusion bodies. (B to D) gE-AYRV-infected xenograft stained with rabbit polyclonal antibody to IE63 (B) and mouse monoclonal antibody to gE (C) and merged image with Hoechst counterstain (D). The white arrow in D indicates the patchy appearance of membrane-associated gE.

lytic infection may not require adaptive immune defenses but requires an "*in vivo*" microenvironment, as VZV infection of cultured neurons or explanted ganglia is rapidly lytic (8).

Our aim was to identify molecular requirements for VZV neuropathogenesis, in particular, viral genetic elements that facilitate productive infection in neurons during primary DRG infection or reactivation from latency. In a previous report, we demonstrated the unexpected finding that requirements for VZV gI are less stringent in neuronal ganglia than in skin (24). Whereas VZV gI was strictly required for skin and T-cell tropism *in vivo*, a gI deletion mutant (rOkaΔgI) was able to replicate in sensory neurons and satellite cells in DRG xenografts, although infectivity was significantly reduced, with a delay in infectious virus production to day 28 after infection (24). The slow infectious process continued for at least 70 days, with limited spread and without any evidence of the transition to viral persistence that occurs in DRG infected with intact VZV.

We observed a similar impairment in early VZV infection in DRG xenografts infected with the gEΔCys mutant. VZV genome copy numbers were significantly reduced in DRG xenografts infected with gEΔCys compared with rOka at 14 days after infection despite a higher-titer virus inoculum. Viral protein expression was absent in neurons and satellite cells at 14 days after infection and was observed only within a few isolated neuron-satellite cell complexes at 28 days after infection. These findings suggest that viral spread within ganglionic cells is extremely inefficient in the absence of the gE/gI interaction. The propagation of VZV in skin tissue and cultured cells is facilitated by cell-cell spread, which requires gE/gI heterodimer formation (2). Dingwell and colleagues previously demonstrated that the HSV gE/gI interaction was critical for HSV transmission through synaptically linked neurons (6). We speculate that the requirement for gE/gI binding in efficient VZV propagation within DRG tissues may reflect an impairment of cell-cell spread from one infected neuron to neighboring neurons or may reflect an altered tropism for specific neuronal subtypes.

During VZV reactivation, the spread of VZV from the reactivating neuron to encapsulating satellite cells may provide a mechanism for viral amplification within the neuron-satellite cell complex that substantially enhances VZV access to the skin. VZV exhibits a marked tropism for satellite cells as well as neurons, whereas HSV replication in satellite cells is restricted (17, 22). The VZV-induced fusion of neuron-satellite cell membranes and the release of virions from satellite cells facilitate the spread of the virus to the adjacent satellite cells that surround the neighboring neurons; VZV transport along axons from these secondarily infected neurons would then increase the delivery of virions to the skin. The capacity to

induce the fusion of satellite cell and neuronal membranes and replicate within satellite cells appears to be unique to VZV and may explain why VZV reactivation induces extensive neuropathological changes within the affected ganglion, whereas HSV reactivation does not. In DRG xenografts infected with gEΔCys and rOkaΔgI, we observed a marked reduction in the capacity for the fusion of neuronal and satellite cell membranes, suggesting a direct role for the gE/gI interaction in this process.

Despite the inefficiency of cell-cell spread and fusion impairment in gEΔCys-infected DRG, overall ganglionic damage was much more severe than that in rOka-infected xenografts. Viral proteins were detected in only a few isolated neuron-satellite cell complexes at 28 days after infection but were abundantly detected at 44 days after infection. By day 56, acellular fibrotic fields were extensive in 8 of 9 DRG; normal-appearing neuronal islets remained in only one DRG infected with the gEΔCys mutant. These rapid pathological changes are markedly more severe than what we observed during the transition to persistence in rOka-infected DRG. The accumulation of misfolded or immature gE, in the absence gI chaperone function, may have toxic effects on ganglionic cells infected with the gEΔCys mutant. The expression of gE alone has lethal effects on cultured cells (12). We also speculate that the long, slow replicative phase of the gEΔCys mutant may result in an overstimulation of cellular pathways that mediate processes such as inflammation, repair, and fibrosis. Necrotic changes were not observed in DRG xenografts that were chronically infected with rOkaΔgI, where the replacement rate of satellite and other nonneuronal cell types may have outpaced the lytic infection of these cells.

Whereas the disruption of the gE interaction with gI had dramatic consequences for neuronal infection, we did not observe any detriment to VZV neuropathogenesis upon the disruption of the interaction between gE and cellular insulin-degrading enzyme (IDE), which was previously proposed to be a cellular receptor for VZV (10). The gEΔ27-90 mutant replicated extensively within DRG xenografts, causing significant cytopathic effects and VZV genome copy numbers that approached those achieved by rOka. Since IDE was expressed prominently on sensory neurons within DRG xenografts, these results indicate that the gE/IDE interaction is not required for VZV neurotropism and that an alternate receptor may participate in VZV entry into cells within neuronal ganglia.

Berarducci et al. previously observed reduced gE synthesis in association with a smaller deletion of aa 27 to 51 and altered gE localization *in vitro* at 72 h after infection with the gEΔ27-90 mutant (2). We observed some difference in the intracellular localization of gE in neurons infected with the gEΔ27-90 mutant compared with that of gE in neurons infected with rOka but no differences in the VZV genome copy number, infectious virus production, or VZV-induced fusion. Polykaryon formation and viral titers in skin xenografts were reduced by mutations within aa 27 to 90, whereas these mutations had no effect on T-cell tropism (3). These tissue-specific differences suggest that the gEΔ27-90 mutant may disrupt other gE functional domains in addition to the gE/IDE interaction, which may be more critical for the characteristic VZV syncytium formation and replication in skin and *in vitro* than tropism for T cells and neurons.

In addition to gE interaction partners, we examined the role of signal-dependent gE trafficking in the VZV replication cycle in sensory neurons. Zhu et al. previously identified an AYRV motif (aa 568 to 571) that directs VZV gE to the TGN; internalization is potentiated by an acidic cluster (SSTT) (9, 25). Earlier work by Moffat et al. demonstrated that an alanine substitution in the SSTT motif enhanced VZV replication *in vitro* but had no effect on replication in skin or T-cell xenografts in SCID mice (14). A mutation of the AYRV motif had no effect on replication or cell-cell spread *in vitro* but significantly impaired replication in skin xenografts and, to a lesser extent, T-cell xenografts *in vivo* (14).

In sensory neurons, both gE AYRV-mediated signaling and phosphorylation at the SSTT domain were dispensable for VZV replication and spread. Neither gE-AYRV nor gE-SSTT showed any impairment in replication compared with rOka when assessed by real-time PCR for viral genomes and infectious virus production. Both viruses caused a significant cytopathic effect, and virus release within 14 days after infection and VZV genome copy numbers did not differ significantly at 14 and 28 days after infection. It is possible that gE phosphorylation at the SSTT site does not potentiate TGN internalization in sensory neurons; the endodomain contains other potential S/T phosphorylation sites that may substitute for the mutated sites. We detected reduced gE expression in IE63-negative neurons at 14 days after infection and low levels of gB transcripts in gE-AYRV-infected DRG at 56 days after infection, when the viral transcription of glycoproteins is normally silenced. This finding suggests that the reduced cell surface expression of gE may delay the activation of viral or host factors that facilitate the transition to long-term persistence.

Taken together, our observations suggest that there are differential requirements for the gE/gI interaction, the gE/IDE interaction, and gE internalization in sensory nerve ganglia compared to those in skin. Moreover, the gE/gI interaction is important for early VZV neurovirulence. HSV and PRV mutants lacking gE or gE/gI heterodimer formation exhibit decreased neurovirulence and spread in animal models and cultured neurons (6, 7, 19–21). As we have previously observed with a gI deletion mutant, our experiments with VZV gE mutants show that changes that produce neuroattenuation initially may have unpredicted consequences as infection progresses. We have not observed the severe cytopathic changes in DRG infected with the mutant that blocks the gE interaction with gI when other VZV mutants were evaluated in DRG (24). An understanding of tissue-specific differences in VZV pathogenesis is important to further our understanding of the specific molecular requirements for VZV neurotropism and latency. Defining genes that contribute to VZV neurovirulence has direct relevance for the design of neuroattenuated varicella vaccines.

ACKNOWLEDGMENTS

This work was supported by grants AI20459 and AI053846 from the National Institute of Allergy and Infectious Diseases and grant CA049605 from the National Cancer Institute.

We thank Xibing Che for generous assistance with animal surgery, Mike Reichelt and Preeti Sikka for technical support, Marvin Sommer and Jennifer Moffat for construction and characterization of gE AYRV and SSTT recombinant viruses, and Raymond Sobel for valuable discussions.

REFERENCES

1. **Berarducci, B., M. Ikoma, S. Stamatis, M. Sommer, C. Grose, and A. M. Arvin.** 2006. Essential functions of the unique N-terminal region of the varicella-zoster virus glycoprotein E ectodomain in viral replication and in the pathogenesis of skin infection. J. Virol. **80:**9481–9496.
2. **Berarducci, B., J. Rajamani, M. Reichelt, M. Sommer, L. Zerboni, and A. M. Arvin.** 2009. Deletion of the first cysteine-rich region of the varicella-zoster virus glycoprotein E ectodomain abolishes the gE and gI interaction and differentially affects cell-cell spread and viral entry. J. Virol. **83:**228–240.
3. **Berarducci, B., J. Rajamani, L. Zerboni, X. Che, M. Sommer, and A. M. Arvin.** 2010. Functions of the unique N-terminal region of glycoprotein E in the pathogenesis of varicella-zoster virus infection. Proc. Natl. Acad. Sci. U. S. A. **107:**282–287.
4. **Chaudhuri, V., M. Sommer, J. Rajamani, L. Zerboni, and A. M. Arvin.** 2008. Functions of varicella-zoster virus ORF23 capsid protein in viral replication and the pathogenesis of skin infection. J. Virol. **82:**10231–10246.
5. **Cohen, J., S. Straus, and A. Arvin (ed.).** 2006. Varicella-zoster virus replication, pathogenesis and management, 5th ed. Lippincott-Raven, Philadelphia, PA.
6. **Dingwell, K. S., L. C. Doering, and D. C. Johnson.** 1995. Glycoproteins E and I facilitate neuron-to-neuron spread of herpes simplex virus. J. Virol. **69:** 7087–7098.
7. **Enquist, L. W., M. J. Tomishima, S. Gross, and G. A. Smith.** 2002. Directional spread of an alpha-herpesvirus in the nervous system. Vet. Microbiol. **86:**5–16.
8. **Gowrishankar, K., B. Slobedman, A. L. Cunningham, M. Miranda-Saksena, R. A. Boadle, and A. Abendroth.** 2007. Productive varicella-zoster virus infection of cultured intact human ganglia. J. Virol. **81:**6752–6756.
9. **Kenyon, T. K., J. I. Cohen, and C. Grose.** 2002. Phosphorylation by the varicella-zoster virus ORF47 protein serine kinase determines whether endocytosed viral gE traffics to the trans-Golgi network or recycles to the cell membrane. J. Virol. **76:**10980–10993.
10. **Li, Q., M. A. Ali, and J. I. Cohen.** 2006. Insulin degrading enzyme is a cellular receptor mediating varicella-zoster virus infection and cell-to-cell spread. Cell **127:**305–316.
11. **Mallory, S., M. Sommer, and A. M. Arvin.** 1997. Mutational analysis of the role of glycoprotein I in varicella-zoster virus replication and its effects on glycoprotein E conformation and trafficking. J. Virol. **71:**8279–8288.
12. **Mo, C., E. E. Schneeberger, and A. M. Arvin.** 2000. Glycoprotein E of varicella-zoster virus enhances cell-cell contact in polarized epithelial cells. J. Virol. **74:**11377–11387.
13. **Moffat, J., H. Ito, M. Sommer, S. Taylor, and A. M. Arvin.** 2002. Glycoprotein I of varicella-zoster virus is required for viral replication in skin and T cells. J. Virol. **76:**8468–8471.
14. **Moffat, J., C. Mo, J. J. Cheng, M. Sommer, L. Zerboni, S. Stamatis, and A. M. Arvin.** 2004. Functions of the C-terminal domain of varicella-zoster virus glycoprotein E in viral replication in vitro and skin and T-cell tropism in vivo. J. Virol. **78:**12406–12415.
15. **Niizuma, T., L. Zerboni, M. H. Sommer, H. Ito, S. Hinchliffe, and A. M. Arvin.** 2003. Construction of varicella-zoster virus recombinants from parent Oka cosmids and demonstration that ORF65 protein is dispensable for infection of human skin and T cells in the SCID-hu mouse model. J. Virol. **77:**6062–6065.
16. **Polcicova, K., K. Goldsmith, B. L. Rainish, T. W. Wisner, and D. C. Johnson.** 2005. The extracellular domain of herpes simplex virus gE is indispensable for efficient cell-to-cell spread: evidence for gE/gI receptors. J. Virol. **79:** 11990–12001.
17. **Reichelt, M., L. Zerboni, and A. M. Arvin.** 2008. Mechanisms of varicella-zoster virus neuropathogenesis in human dorsal root ganglia. J. Virol. **82:** 3971–3983.
18. **Shi, S. R., R. J. Cote, and C. R. Taylor.** 1997. Antigen retrieval immunohistochemistry: past, present, and future. J. Histochem. Cytochem. **45:**327–343.
19. **Tirabassi, R. S., and L. W. Enquist.** 2000. Role of the pseudorabies virus gI cytoplasmic domain in neuroinvasion, virulence, and posttranslational N-linked glycosylation. J. Virol. **74:**3505–3516.
20. **Wang, F., W. Tang, H. M. McGraw, J. Bennett, L. W. Enquist, and H. M. Friedman.** 2005. Herpes simplex virus type 1 glycoprotein E is required for axonal localization of capsid, tegument, and membrane glycoproteins. J. Virol. **79:**13362–13372.
21. **Wang, F., E. E. Zumbrun, J. Huang, H. Si, L. Makaroun, and H. M. Friedman.** 2010. Herpes simplex virus type 2 glycoprotein E is required for efficient virus spread from epithelial cells to neurons and for targeting viral proteins from the neuron cell body into axons. Virology **405:**269–279.
22. **Wilkinson, R., C. Leaver, A. Simmons, and R. A. Pereira.** 1999. Restricted replication of herpes simplex virus in satellite glial cell cultures clonally derived from adult mice. J. Neurovirol. **5:**384–391.
23. **Zerboni, L., C. C. Ku, C. D. Jones, J. L. Zehnder, and A. M. Arvin.** 2005. Varicella-zoster virus infection of human dorsal root ganglia in vivo. Proc. Natl. Acad. Sci. U. S. A. **102:**6490–6495.
24. **Zerboni, L., M. Reichelt, C. D. Jones, J. L. Zehnder, H. Ito, and A. M. Arvin.** 2007. Aberrant infection and persistence of varicella-zoster virus in human dorsal root ganglia in vivo in the absence of glycoprotein I. Proc. Natl. Acad. Sci. U. S. A. **104:**14086–14091.
25. **Zhu, Z., Y. Hao, M. D. Gershon, R. T. Ambron, and A. A. Gershon.** 1996. Targeting of glycoprotein I (gE) of varicella-zoster virus to the trans-Golgi network by an AYRV sequence and an acidic amino acid-rich patch in the cytosolic domain of the molecule. J. Virol. **70:**6563–6575.